ELSEVIER

Neurobiology of Aging 33 (2012) 1533–1544

NEUROBIOLOGY OF AGING

www.elsevier.com/locate/neuaging

Gadolinium-staining reveals amyloid plaques in the brain of Alzheimer's transgenic mice

Alexandra Petiet[a,b,c,d], Mathieu Santin[a,b,c], Anne Bertrand[b,c], Christopher J. Wiggins[d], Fanny Petit[b,c], Diane Houitte[b,c], Philippe Hantraye[b,c], Jesus Benavides[a], Thomas Debeir[a], Thomas Rooney[a], Marc Dhenain[b,c,d,*]

[a] *Sanofi-aventis, Aging Therapeutic Strategic Unit, Chilly-Mazarin, France*
[b] *CNRS, URA 2210, Fontenay aux Roses, France*
[c] *CEA, I2BM, MIRCen, Fontenay aux Roses, France*
[d] *CEA, I2BM, Neurospin, Gif-sur-Yvette, France*

Received 31 March 2010; received in revised form 3 March 2011; accepted 11 March 2011

Abstract

Detection of amyloid plaques in the brain by in vivo neuroimaging is a very promising biomarker approach for early diagnosis of Alzheimer's disease (AD) and evaluation of therapeutic efficacy. Here we describe a new method to detect amyloid plaques by in vivo magnetic resonance imaging (MRI) based on the intracerebroventricular injection of a nontargeted gadolinium (Gd)-based contrast agent, which rapidly diffuses throughout the brain and increases the signal and contrast of magnetic resonance (MR) images by shortening the T1 relaxation time. This gain in image sensitivity after in vitro and in vivo Gd staining significantly improves the detection and resolution of individual amyloid plaques in the cortex and hippocampus of AD transgenic mice. The improved image resolution is sensitive enough to demonstrate an age-dependent increase of amyloid plaque load and a good correlation between the amyloid load measured by μMRI and histology. These results provide the first demonstration that nontargeted Gd staining can enhance the detection of amyloid plaques to follow the progression of AD and to evaluate the activity of amyloid-lowering therapeutic strategies in longitudinal studies.

Keywords: Alzheimer; Amyloid; Biomarker; Contrast agent; MRI; Gadolinium

1. Introduction

The formation of senile plaques composed of aggregated extracellular deposits of β-amyloid (Aβ) is 1 of the major neuropathological hallmarks of Alzheimer's disease (AD). The development of in vivo neuroimaging techniques to noninvasively detect amyloid plaques in the brain is a very promising approach for an earlier diagnosis of AD and can be used to evaluate the efficacy of antiamyloid therapies in clinical trials. The ability to image amyloid load could also provide a translational biomarker for longitudinal pharmacological studies in animal models and clinical trials.

Histological stains have been developed to detect amyloid plaques on brain sections. Besides this conventional postmortem technique, most neuroimaging studies of amyloid load in humans have been performed with positron emission tomography (PET) and several ligands have been developed that can detect amyloid in human brains (Klunk et al., 2004; Nordberg, 2007). However, the low spatial resolution of PET does not allow the visualization of individual plaques. Studies in animals have provided controversial results with some data suggesting that PET ligands such as the Pittsburgh compound B (PiB) can detect amyloid plaques (Maeda et al., 2007), while some other reports suggested that plaques are not detected by these ligands

* Corresponding author at: MIRCen, CEA/CNRS URA 2210, 18 Route du Panorama, 92265 Fontenay aux Roses, France. Tel.: +33 (0)1 46 54 81 92; fax: +33 (0)1 46 54 84 51.
E-mail address: marc.dhenain@cea.fr (M. Dhenain).

0197-4580/$ – see front matter © 2012 Elsevier Inc. All rights reserved.
10.1016/j.neurobiolaging.2011.03.009

(Klunk et al., 2005). Various other imaging modalities have been developed to detect amyloid plaques (see Delatour et al., 2010 and Dhenain, 2008 for reviews). For example, optical imaging dyes such as AOI987, an oxazine dye, have been demonstrated to readily penetrate the intact blood-brain barrier (BBB) and to bind to amyloid plaques (Hintersteiner et al., 2005). Using near-infrared optical imaging, a specific interaction of AOI987 with amyloid plaques was shown in mice in vivo, and confirmed by postmortem analysis of brain slices.

Only neuroimaging studies based on magnetic resonance imaging (MRI) have detected individual amyloid plaques in human brain samples (Meadowcroft et al., 2009) and in mouse models (Chamberlain et al., 2009; Dhenain et al., 2009; Jack et al., 2004). Several approaches have been evaluated based on the natural contrast of the plaques or with dedicated targeted contrast agents. The plaques appear as dark spots in T2, T2*-weighted (T2*w) or susceptibility-weighted images because of the presence of iron in the core of these lesions. However, in humans, the possibility to detect iron within plaques has been controversial (Dhenain et al., 2002; Meadowcroft et al., 2009). Also, iron accumulation in mice mainly occurs in old animals, which makes amyloid plaque detection very challenging in young animals. Using magnetic resonance (MR) contrast agents can be another option to detect amyloid plaques with MRI. One study using a fluorine-based MR contrast agent has been reported to detect amyloid plaques following intravenous injection of the agent in mice (Higuchi et al., 2005). Some other studies have been successful for early stage detection of amyloid plaques thanks to amyloid peptides tagged with MR contrast agents (gadolinium chelates or monocrystalline iron oxide nanoparticles) in combination with compounds like mannitol that allow the contrast agent to cross the BBB (Poduslo et al., 2002; Sigurdsson et al., 2008; Wadghiri et al., 2003). However, these methods are technically difficult and still require extensive validation.

Staining tissue samples with gadolinium (Gd) chelates has previously been used to increase the signal- and contrast-to-noise ratios in MR images of whole mice (Johnson et al., 2002) or of brains (Benveniste et al., 2000; Dhenain et al., 2006; Kappeler et al., 2007). These protocols were based on the administration of a Gd chelate and formalin by intracardiac perfusion (active staining; Johnson et al., 2002) or by immersion of tissues in the Gd solution (passive staining; Dhenain et al., 2006). In the present study, we describe a new Gd staining method based on the injection of a nontargeted Gd agent into the cerebral ventricles that significantly improves the in vivo detection of amyloid plaques by μMRI in the brain of an APP/PS1 transgenic mouse model of amyloidosis (Blanchard et al., 2003). This method may also be applicable to detect amyloid plaques and evaluate the activity of antiamyloid agents in longitudinal studies in the same animals.

2. Methods

2.1. Animals

Experiments were conducted on female APP/PS1 transgenic (Tg) mice overexpressing amyloid precursor protein (APP) and presenilin 1 (PS1) mutations associated with familial AD (double Thy1 APP751 SL Swedish (KM670/671NL) and London (V717I) mutations introduced in the human APP751 sequence × HMG PS1 M146L transgenic mouse line) (Blanchard et al., 2003; Delatour et al., 2006). In these animals, amyloid deposition starts at the age of 2.5 months (Blanchard et al., 2003). Amyloid-free PS1 females were used as controls. In vivo images were recorded for 4 groups of animals at ages (± 1 week) of 6, 9, 14, and 20 months. Six animals were followed longitudinally and were injected at 2 time points: 4 animals were first injected at 3.5 months and then at 8 months; 2 animals were first injected at 14.5 months and then at 17.5 months. Fourteen additional animals were used to evaluate neuroinflammation and animal weight up to 42 days following intracerebroventricular injection (ICV) of gadolinium. A total of 36 animals were used for this study (19 APP/PS1 and 17 PS1 controls).

2.2. Surgical procedure

The animals were anesthetized with an intraperitoneal (i.p.) injection of a mixture of ketamine, 10 mg kg^{-1} (Imalgène® 500, Merial, Lyon, France) and medetomidine 0.68 mg/kg (Domitor®, Pfizer Santé Animale, Paris, France). After their heads were shaved, the mice were placed on a stereotaxic frame using ear bars and a tooth bar to hold them still. A heating pad was used to keep them at physiological temperature throughout the procedure. After a midline incision into the skin, the coordinates of the bregma were recorded for anterior-posterior (A/P) and lateral (L) references. The skull was bilaterally perforated with a Dremel at coordinates A/P -0.2 mm and L ± 1 mm, according to a stereotaxic atlas (Paxinos and Franklin, 2001). Blunt Hamilton syringes were used to inject gadoterate meglumine (Gd-DOTA, DOTAREM®, Guerbet, Aulnay-sous-Bois, France) into the lateral ventricles at coordinate -1.8 mm relative to the surface of the dura mater. A total volume of 1 μL (0.5 μmol) was injected in each side at a rate of 0.2 μL/minute. Upon completion of the injections, the needles were very slowly withdrawn to minimize any outflow from pressure release and the skin was then sutured back. The anesthesia was reversed using atipamezole hydrochloride (Antisedan®, Pfizer) at a dose of 10 mg/kg to allow recovery before μMR imaging.

The effect of injection on animal's physiology was further evaluated by monitoring the weight of 17-month-old PS1 mice over 42 days after ICV injection of gadolinium ($n = 6$) or saline ($n = 6$).

2.3. In vivo MRI experiments

In vivo μMRI studies were performed on a 7-Tesla spectrometer (Pharmascan, Bruker Biospin, Ettlingen, Germany) equipped with a 9-cm inner diameter gradient system (strength of 760 mT/m and slew rate of 6836 T/m/s) and interfaced to a console running Paravision 5.0. A birdcage coil (Bruker Biospin GmbH) of diameter = 38 mm was used for transmit-receive. A 3D gradient-echo sequence (FLASH) was used to record T2*w images with repetition time (TR) = 32 ms, echo time (TE) = 16 ms, flip angle (FA) = 20°, receiver bandwidth (Bw) = 12.5 kHz, matrix (Mtx) = 332 × 332 × 64, field of view (FOV) = 15 × 15 × 10 mm^3, yielding a resolution of 45.2 × 45.2 × 156 μm^3, number of averages (Nex) = 10, for a total acquisition time (Tacq) of 1 hour, 54 minutes. The images were 0-filled to 664 × 664 × 128 pixels resulting in an extrapolated resolution of 22.6 × 22.6 × 78 μm^3. Values of signal-to-noise ratio (SNR; tissue signal intensity over standard deviation of the background noise) were calculated over the whole brains on midcoronal slices. Contrast-to-noise ratios (CNRs; signal difference between 2 tissues over standard deviation of the background noise) between the cortex and the white matter and between the parenchyma and the amyloid plaques were also calculated. Complementary experiments, including longitudinal studies, with an optimized receive-only surface coil (2-channel mouse brain surface ^{1}H coil, RapidBiomed GmbH, Rimpar, Germany) were performed on a 7-T Varian system (rodent gradient set of 700 mT/m). T2*w images (TR = 50 ms, TE = 25 ms, FA = 20, Bw = 12.5 kHz, FOV = 15 × 15 × 15 mm^3, Nex: 2, matrix = 512 × 512 × 128) were recorded with a resolution as high as 29 × 29 × 117 μm^3 and acquisition time of only 1 hour, 49 minutes.

During the μMRI scans the animals were anesthetized with isoflurane (5% for induction, 0.75%–1.5% for maintenance) and air (1.5 L/minute), administered via a facemask. Respiration rate was monitored to ensure animal stability until the end of the experiment. The body temperature was maintained at 37 ± 1 °C with a circulating water-filled heating blanket connected to a thermoregulated water bath and rectal temperature was monitored throughout the experiments.

2.4. In vitro MRI experiments

Following the in vivo experiments, the animals were administered a high dose of pentobarbital sodium (100 mg/kg) and then perfusion-fixed with 10% buffered formalin. The brains were excised and immersed in formalin for further fixation at 4 °C for at least 24 hours. We adapted and optimized the previously published "staining" protocols (Dhenain et al., 2006; Petiet et al., 2007) to Gd-stain the fixed brains: the samples were soaked in a solution of phosphate buffered saline (PBS) and 0.5 M gadoterate meglumine at a dilution of 1:200 (2.5 mM) and stored at 4 °C for at least 24 hours prior to imaging. For scanning, the brains were placed in a tight plastic tube filled with Fluorinert® (3 M™, Cergy-Pontoise, France), an aprotonic perfluorocarbon-based fluid that provides a black background in MR images.

In vitro studies were performed on a clinical 7-Tesla spectrometer (Syngo MR, VB15, Siemens Medical Solutions, Erlangen, Germany), equipped with an AC84 head gradient set with 36-cm available bore (strength of 80 mT/m and slew rate of 333 mT/m/s). A home-built birdcage coil (inner diameter = 24 mm) was used for transmit-receive. A 3D gradient-echo sequence was used (FLASH) to acquire T2*w images (TR = 100 ms, TE = 21 ms, FA = 25°, Bw = 50 Hz/pixel, Nex = 6, matrix = 1024 × 864, FOV = 24 × 20.25 mm^2, slice thickness = 0.09 mm, yielding a resolution of 23.4 × 23.4 × 90 μm^3 and number of slices = 72 for a total acquisition time of 13 hours, 49 minutes). SNR and CNR were calculated in postmortem samples using the same method as for the in vivo experiments.

2.5. Relaxation time measurements

Relaxation times for both in vivo (n = 2 APP/PS1) and in vitro brains (n = 2 APP/PS1, n = 2 PS1) were measured at 7T on the Bruker system. For T1 measurements, a 2D turbo spin-echo sequence (RARE) was used with 6 TR values (TR = 338, 500, 1000, 2000, 4000, and 8000 ms; TE = 8.3 ms; FOV = 20 × 20 mm^2; matrix = 128 × 128; slice thickness = 0.5 mm; interslice spacing = 0.5 mm and a total of 15 slices in ~12 minutes; RARE factor = 2). The same 2D RARE sequence was used for T2 measurements but with TR = 8000 ms and with 8 values of varying TE from 7 to 105 ms with 14 ms increments in ~6 minutes. For T2* measurements, a 2D multigradient echo sequence was used with TR = 3000 ms and with 12 values of varying TE from 2.8 to 79.8 ms with 7 ms increments in ~4 minutes. The Bruker fit package (ParaVision 5.0) was used to calculate relaxation times from exponential regression curves and to generate parametric maps. Relaxation times were measured from 5 regions of interest (ROIs) drawn on midcoronal slices: thalamus, hippocampus, corpus callosum, cortex, and from the whole brain.

For in vivo experiments, relaxation maps were recorded every 30–40 minutes over 4.5 hours. The first postinjection imaging time point was about 40 minutes after the Gd staining procedure. This was the minimum time to allow for animal recovery after anesthesia reversal and before isoflurane induction, and for animal setup in the magnet. The last time point was recorded 24 hours postinjection. For in vitro samples, relaxation times were measured before and after the passive staining procedure.

2.6. Amyloid load quantification from MR sections

Cortical amyloid load was calculated for both in vivo and in vitro datasets by using a method similar to that reported by Jack et al. (2005). A total of 144 and 112 ROIs per

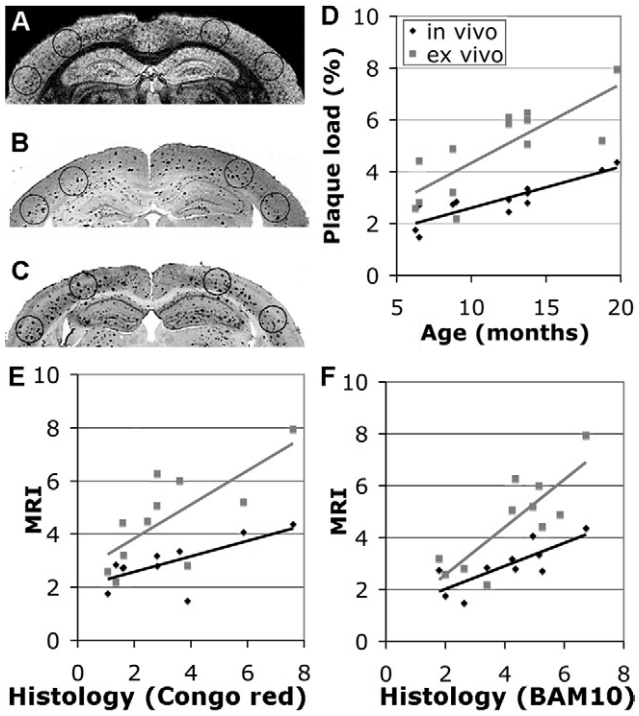

Fig. 1. Regions of interest (ROIs) over which the measurements were performed and amyloid load quantification from gadolinium (Gd)-stained magnetic resonance imaging (MRI) and histological sections. Two cortical regions of interest per hemisphere were selected in several magnetic resonance (MR) slices (A) and in several Congo red (B) and BAM10 histological sections (C) to count the number of plaques per ROI. The plaque load measured with μMRI shows a correlation with age (D). The brain plaque load measured with μMRI also correlates with Congo red staining (E) and with BAM10 immunohistochemistry (F).

animal were analyzed for in vivo and in vitro samples, respectively: 36 or 28 slices evenly spaced by 780 μm or 450 μm, were selected and 4 circular ROIs (diameter ~900 μm) were drawn on each of these slices (2 in each hemisphere) (Fig. 1A). Hypointense spots were manually counted, excluding hypointense elements that could be followed over more than 2 adjacent slices, or that had a tube-like shape, suggesting the presence of a blood vessel. Areas of several hypointense spots were measured in each ROI. Plaque load was determined as the ratio of the mean area of the hypointense spots multiplied by the number of spots counted over the area of the ROI.

2.7. Neuropathology

After imaging, the brains of the animals evaluated in a cross-sectional way were cryoprotected in sucrose (15% for 24 hours then 30% for 24 hours) and cut into 40-μm thick coronal sections on a freezing microtome. The sections were stained for β-amyloid deposits (anti-β-amyloid immunohistochemistry and Congo red) to quantify the amyloid load and were also stained for iron deposits (Perls-DAB stain). For anti-β-amyloid immunohistochemistry, the sections were first rinsed in phosphate-buffered saline (PBS 0.1 M) and in 30% hydrogen peroxide. They were then pretreated with 0.2% octylphenol ethylene oxide condensate (Triton X-100™, Sigma, St. Louis, MO, USA). After this pretreatment, they were incubated with an anti-β-amyloid primary antibody (monoclonal BAM10 clone A3981, dilution 1:1000, Sigma-Aldrich®) for 48 hours and then with a secondary antibody (biotinated immunoglobulin G [IgG] anti-mouse, BA-9200, dilution 1:1000, Vector® Labs, Burlingame, CA, USA) for 1 hour. Before revelation (VIP substrate kit for peroxidase, Vector® Labs) the reaction was amplified for 1 hour with a biotin-avidin complex (ABC Vectastain kit, Vector® Labs) (Berghorn et al., 1994). For Congo red staining, the sections were immersed in an 80% ethanol solution saturated with Congo red (Fluka 60910, Sigma-Aldrich®) and sodium chloride for 30 minutes. For Perls staining (El Tannir El Tayara et al., 2006), endogenous peroxidases were first inactivated by immersion in a methanol/H_2O_2 solution. The sections were then stained with 2% potassium ferrocyanide (P9387, Sigma-Aldrich®) and 2% hydrogen chloride for 20 minutes. Iron staining was finally intensified using diaminobenzidine (DAB) (1 g/L), Tris (0.2 M), and 30% hydrogen peroxide for 20 minutes. All sections were digitized using a microscope (Axioplan-1™, Zeiss Inc., Thornwood, NY, USA) connected to a digital camera (Microfire™, Optronics Inc., Goleta, CA, USA).

To evaluate the neuroinflammation induced by Gd injection in mice, the brain of 2 APP/PS1 8-month-old animals injected 2 times, at 3.5 and 8 months and 2 age-matched APP/PS1 animals that did not receive any injection were also compared using double immunofluorescence staining against amyloid plaques and reactive astrocytes or microglial cells. Sections were first rinsed in phosphate-buffered saline (PBS 0.1 M) and then incubated in 0.2% Triton X-100, 4.5% normal goat serum in PBS 0.1 M for 30 minutes. Section were then incubated overnight in a mix solution of 2 primary antibodies (monoclonal BAM10 clone A3981; dilution 1/500, Sigma-Aldrich®) and polyclonal glial fibrillary acidic protein (GFAP; dilution 1/10,000, Dako, Glostrup, Denmark) or polyclonal Iba1 (dilution 1/500, Wako®, Osaka, Japan), followed by incubation in a solution of secondary goat anti-mouse IgG coupled to the fluorescent marker Alexa 488 (1:200) and secondary goat anti-rabbit IgG coupled to the fluorescent marker Alexa 594 (1:200) for 1 hour. Sections were mounted on slides and coverslipped with Fluorosave™ reagent (Calbiochem, Darmstadt, Germany). Fluorescent sections were observed using a DM 6000 Leica microscope connected to a camera (Hamamatsu Photonics France, Massy, France).

2.8. Quantification from histological sections

For amyloid load quantification, the immunohistochemically and Congo red stained sections were scanned at a 1200 dpi in-plane resolution (pixel size 0.5 μm) using a flatbed scanner (ImageScanner III, G.E. Healthcare, Orsay,

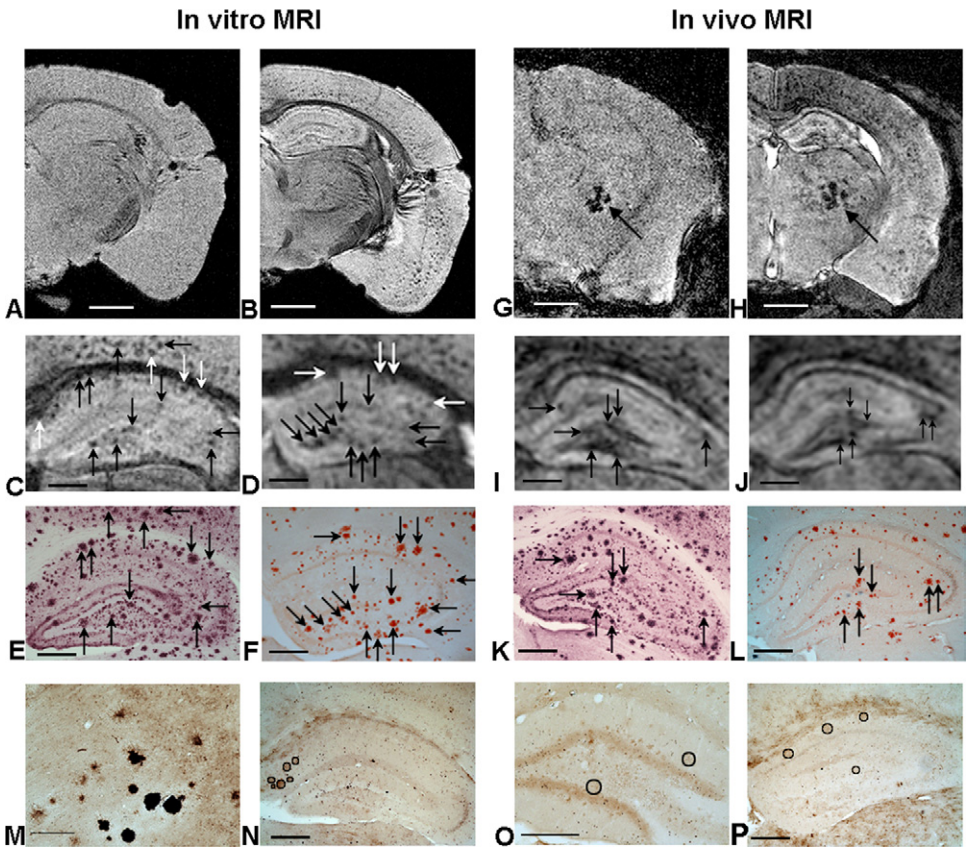

Fig. 2. Amyloid plaque detection after gadolinium (Gd)-staining of a 14-month-old APP/PS1 mouse brain. After in vitro Gd staining (A–D), the image quality was significantly improved (A vs. B) such that hypointense spots could be identified in the cortex and hippocampus. These hypointense spots (arrows in C and D) colocalized with amyloid deposits detected by BAM10 immunohistochemistry (E) and Congo red (F) section staining. After in vivo Gd staining (G–J), the signal and contrast improvements revealed similar hypointense spots (arrows in I and J) that also colocalized with BAM10 (K) and Congo red (L) stainings. The Perls-DAB stainings showed strong iron accumulation within some thalamic plaques (M, 14-month-old APP/PS1 mouse) and lower iron accumulation in the subiculum (circles in N, 20-month-old APP/PS1 mouse). Hippocampal plaques showed only very light iron accumulation at 14 months (O) and at 20 months (P). Note that on in vitro and in vivo images (arrows on G and H) only thalamic plaques were visible both before and after Gd staining. Scale bars on A, B, G, H = 1 mm; scale bars on C–P = 500 μm.

France). Amyloid load was quantified with the same method as for the quantification of amyloid plaques on μMR images (Fig. 1B and C).

2.9. Correlation between in vivo MRI, in vitro MRI, and histology

In vivo and in vitro μMR images and histological sections were manually registered using ImageJ freeware (rsbweb.nih.gov/ij): the μMR images were rotated in 3 directions until the best matching planes with the histology sections were found.

2.10. Statistical analysis

Correlations between amyloid plaque load evaluated by μMRI and histology were based on Pearson's correlation coefficient (Statistica 7.1; StatSoft, Inc., Tulsa, OK, USA). A value of $p < 0.05$ was considered statistically significant.

3. Results

3.1. Gd staining improves detection of amyloid plaques by MRI

In vivo Gd staining of the brain of APP/PS1 and control mice was performed by injecting gadoterate meglumine into the lateral ventricles of the mice. In vitro Gd staining (or passive staining) was obtained by soaking the fixed brains in a solution of PBS and 0.5 M gadoterate meglumine at a dilution of 1:200 (2.5 mM) for at least 24 hours prior to imaging. Fig. 2 shows representative images recorded before (Fig. 2A and G) and after (Fig. 2B and H) in vitro and in vivo Gd staining of a 14-month-old APP/PS1 mouse brain. After Gd staining, several hypointense spots could be detected in the cortex and hippocampus of APP/PS1 mice. Without Gd staining, the images did not show any hypointense spots except in the thalamus (arrows in Fig. 2G and H). The cortical and hippocampal hypointense spots observed after Gd staining were identified as amyloid deposits

Table 1
SNR and CNR measurements before and after in vitro and in vivo Gd staining

	In vitro		In vivo	
	Before Gd staining	After Gd staining	Before Gd staining	After Gd staining
SNR whole grain	2.9 ± 0.6	8.8 ± 2.9	7.8 ± 1.4	16.2 ± 1.0
CNR wm/gm	0.7 ± 0.2	8.0 ± 2.2	1.5 ± 0.9	3.3 ± 1.7
CNR plaques parenchyma	—	7.6 ± 2.6	—	4.8 ± 0.9

Measurements were performed in 14-month-old APP/PS1 mice.
Key: CNR, contrast-to-noise ratio; Gd, gadolinium; gm, gray matter; SNR, signal-to-noise ratio; wm, white matter.

by coregistering the in vitro and in vivo images with Congo red and Aβ-stained histological sections (Fig. 2C–F and I–L). In our experiments, Perls-DAB staining detected iron within the plaques mainly in the thalamus (Fig. 2M, and see Dhenain et al., 2009; El Tannir El Tayara et al., 2007) and in the subiculum (Fig. 2N), 2 brain regions known to be highly loaded with iron (El Tannir El Tayara et al., 2006). Only slight iron staining was detected within a few cortical and hippocampal plaques in animals older than 14 months (Fig. 2O and P). This indicates that most of the hypointense spots detected by μMRI were colocalized with iron-free amyloid plaques.

Gd staining increased the SNR and CNR of the in vitro and in vivo brain images (Table 1). For example, in the in vitro images the SNR from the whole brain and the CNR between the gray and the white matter were increased ~3-fold and ~12-fold, respectively. In the in vivo images, the SNR and the CNR were both increased ~2-fold. The increased SNR and CNR could be explained by changes in the relaxation times caused by the Gd administration. Indeed, it has been previously shown (Dhenain et al., 2006; Petiet et al., 2007) that "passive staining" shortens the T1 of in vitro samples. Fig. 3A shows that the T1 dropped over the whole brain (from ~1500 ms to ~200 ms). The T2 (Fig. 3B) and the T2* (Fig. 3C) shortenings were less severe (from ~37 ms to ~32 ms and from ~27 ms to ~23 ms, respectively). Similarly, in vivo Gd staining shortened all 3 relaxation times relative to the preinjection values 40 minutes after Gd injections and remained low for at least 3 hours (Fig. 3D–F). Over the whole brain, the T1 shortened from ~1750 ms before injection to ~210 ms after injection. Similarly, the T2 and T2* values decreased from ~45 ms and 28 ms, respectively, before injection to ~25 ms and 10 ms after injection. All 3 relaxation times reached minimal values of T1 = 204 ms, T2 = 25 ms, and T2* = 8.6 ms at 80 minutes. Twenty-four hours after injection, the relaxation times had all fully recovered to their initial values (T1 ~1780 ms, T2 ~43 ms, and T2* ~23 ms). This suggests that the contrast agent was cleared out of the brain within 24 hours.

3.2. Quantification and correlation of amyloid plaques detected by MRI and histology

APP/PS1 mice were examined with in vivo and in vitro Gd staining at the ages of 6, 9, 14, and 20 months. The excellent image quality and high resolution of 23 × 23 × 90 μm^3 achieved for in vitro brains allowed us to clearly visualize an age-related increase of plaque density (Fig. 4A–E). In the in vivo images, the signal and contrast enhancement and the 45 × 45 × 156-μm^3 resolution were also sufficient to quantify a similar increase in plaque load (Fig. 4F–J). Fig. 1A–C shows the ROIs over which the measurements were performed. Fig. 1D–F shows the mean in vivo/in vitro amyloid plaque load measurements with means ± interspecimen standard deviations: 2.0 ± 0.6%/3.3 ± 1.0% at 6 months; 2.8 ± 0.1%/3.4 ± 1.4% at 9 months; 3.1 ± 0.3%/5.8 ± 0.6% at 14 months; and 4.2 ± 0.2%/6.6 ± 1.9% at 20 months. We found a significant

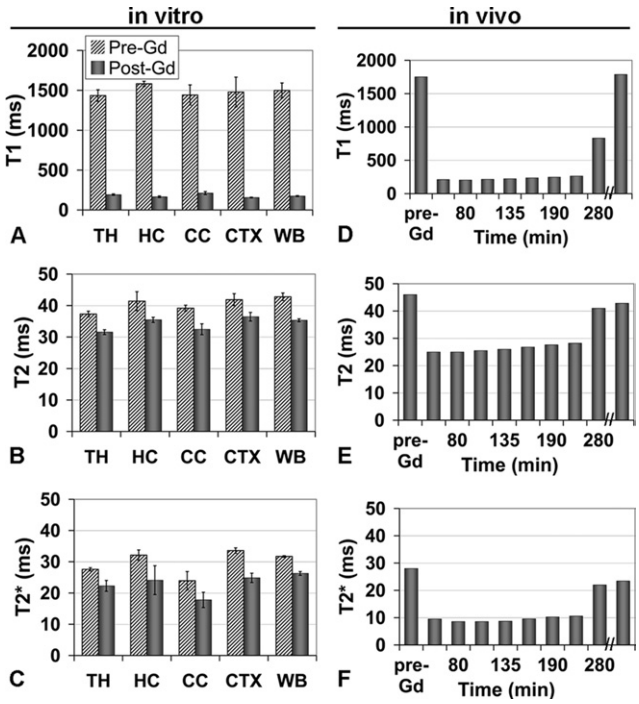

Fig. 3. Effect of gadolinium (Gd) staining on relaxation times T1, T2, and T2*. For in vitro samples, the T1 was significantly reduced (A), whereas the T2 (B) and T2* (C) were only slightly reduced. For in vivo brains, the T1 (D), T2 (E), and T2* (F) were significantly shortened immediately after the injections for about 3.5 hours. At 280 minutes (4.5 hours), all 3 relaxation times started to increase until complete wash out of the Gd at 24 hours (last bar) when they returned to their initial values. The last time point in the in vivo data was recorded at 24 hours postinjection. Error bars represent interspecimen standard deviations. CC, corpus callosum; CTX, cortex; HC, hippocampus; TH, thalamus; WB, whole brain.

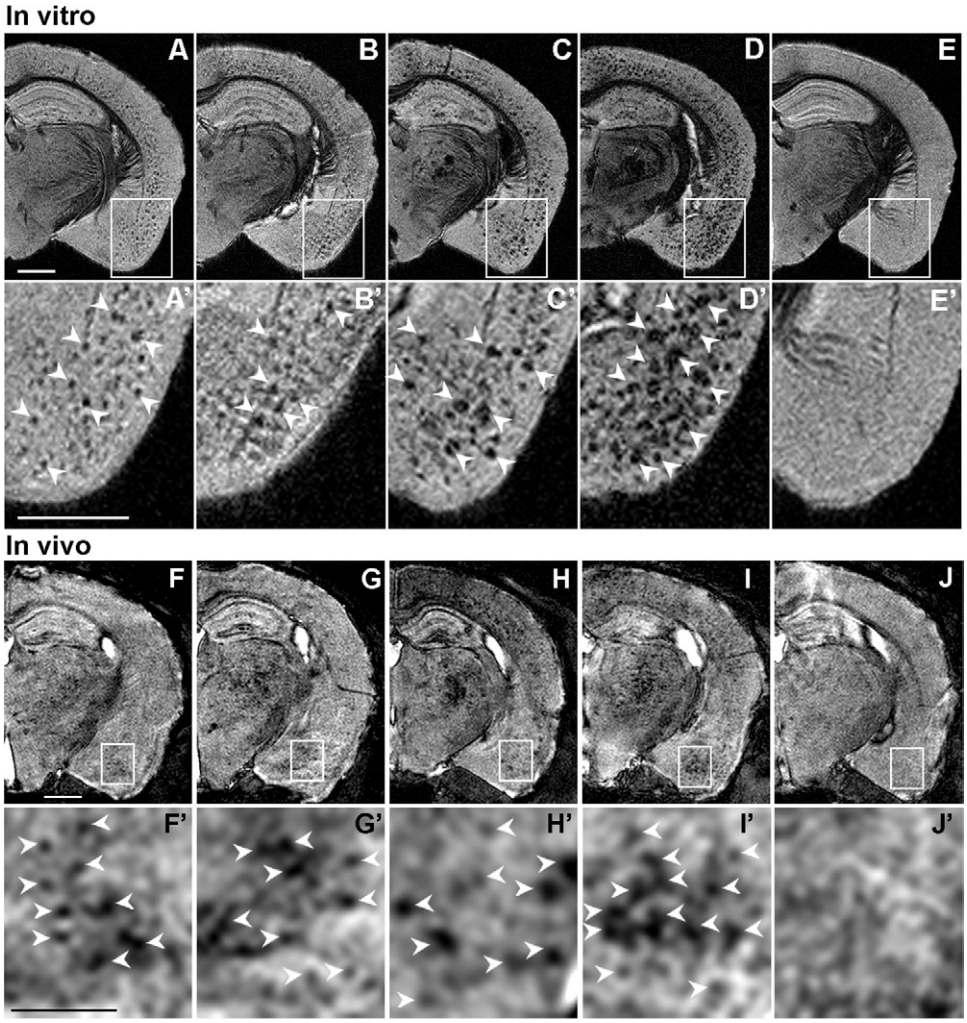

Fig. 4. In vitro and in vivo staining of APP/PS1 mouse brains at 6, 9, 14, and 20 months (from left to right in A–D and F–I, respectively) and of a 14-month-old control PS1 (E and J). Close-up views of the temporal cortex (A'–E' and F'–J'). The APP/PS1 brains showed amyloid plaques (some are indicated with arrowheads in A'–D' and F'–I') but not the PS1 brains (E' and J'). Notice the clear visualization of plaque load increase with age. Scale bars = 1 mm on all images, except on F'–J': scale bar = 500 μm.

correlation between the age of the animals and the amyloid load measured from the in vitro and in vivo μMR images (Fig. 1D: $r = 0.79$, $p < 0.005$, and $r = 0.88$, $p < 0.001$, respectively). Furthermore, the plaque load calculated from the μMR images was also correlated with the amyloid load calculated from the Congo red stained brain sections (Fig. 1E: $r = 0.73$, $p < 0.05$, and $r = 0.69$, $p < 0.05$ for the in vitro and in vivo experiments, respectively) or from BAM10 immunohistochemistry (Fig. 1F: $r = 0.82$, $p < 0.005$ and $r = 0.79$, $p < 0.01$ for the in vitro and in vivo experiments, respectively).

The histology staining allowed the count of very fine plaques of sizes down to 20 μm in diameter. For comparison, after 0-filling, the in vivo MR images had an extrapolated resolution of ~23 μm, same as the in vitro raw datasets. The smallest plaque size detected with both in vivo and in vitro MRI was therefore 45 μm (i.e., 2 pixels), about twice as large as the plaque size measured with histology.

The images previously presented were recorded on a 7T spectrometer, with a 38-mm transmit-receiver coil. Using better coils can greatly improve signal detection, as shown in Fig. 5 where 3D T2*w images were recorded with a receive-only, 2-channel mouse brain surface ^{1}H coil. With this system, a significant gain in SNR allowed us to reach a resolution of $29 \times 29 \times 117$ μm^3 (Fig. 5A: SNR over the whole midcoronal brain slice = 33), which is comparable to the in vitro resolution and also allowed us to record images with a longer TE. This greatly improved individual plaque detection after Gd staining (see arrows in Fig. 5B and a close-up view in Fig. 5C).

Evaluation of animal weight following ICV injection of gadolinium or saline did not highlight any change of weight 2 weeks after injection compared with before injection (Fig. 6B). Because the animals recovered well from the first injection and imaging experiments, we evaluated the feasibility to perform additional imaging studies in the same

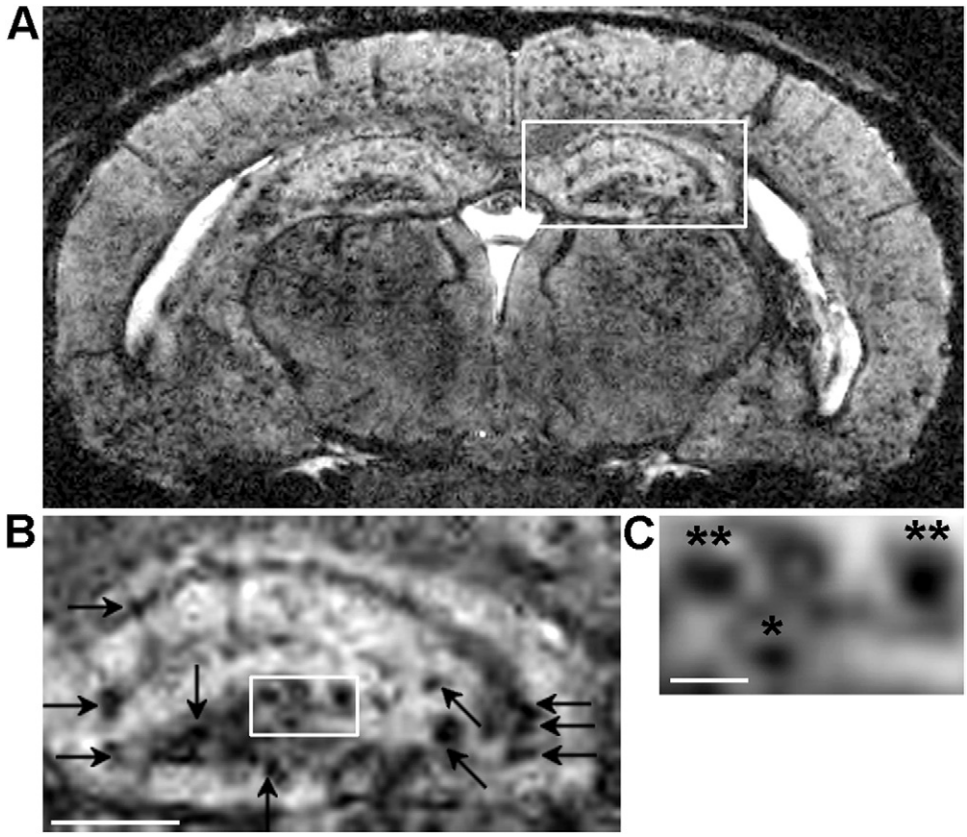

Fig. 5. In vivo magnetic resonance (MR) images of the whole brain (A) and hippocampus (B) of a 12-month-old APP/PS1 mouse after gadolinium (Gd) staining. The T2*w in vivo images were acquired at 29 × 29 × 117 μm^3 with a receive-only, 2-channel mouse brain surface ^1H coil. The very high resolution improved individual plaque detection (some are indicated with arrows). (C) Close-up view of 120 μm large plaques (**) and a 60 μm large plaque (*). Scale bar (B) = 500 μm; scale bar (C) = 300 μm.

animals by reinjecting 6 mice with contrast agent 3 to 5 months after the first injection. Four APP/PS1 mice were injected and imaged at 3.5 months (Fig. 7A) and then again at 8 months (Fig. 7B) and 2 APP/PS1 mice were injected and imaged at 14.5 months (Fig. 7C) and then again at 17.5 months (Fig. 7D). Signal and contrast enhancements following the second Gd staining procedure were similar to those obtained during the first Gd injection, and plaques could therefore be detected. The measurements showed a plaque load increase from 0% to 5.5% from 3.5 to 8 months and from 6.2% to 9.7% from 14.5 to 17.5 months (Fig. 7E). Also, comparison of histological sections stained for amyloid plaques and astrocyte or microglial cells did not highlight any change between the mice Gd-injected twice at 3.5 and 8 months and noninjected mice (Fig. 6A). These results demonstrate that in vivo Gd staining can be used to quantify amyloid plaque load in longitudinal studies.

4. Discussion

In the present study we have described a new method that significantly improves the ability to detect amyloid plaques in the brain of AD transgenic mice by μMRI. This method is based on the intraventricular injection of a nontargeted Gd-based contrast agent that rapidly diffuses throughout the brain and increases the SNR and CNR of MR images by at least 2-fold in all major brain areas by shortening the T1 relaxation time. Through this gain in image sensitivity we have been able to detect individual amyloid plaques after in vitro and in vivo Gd staining in brain areas, such as the cortex and hippocampus, which are known to be particularly sensitive to amyloid plaque formation in human and AD transgenic mice. Interestingly, in the strain of mice that were used, amyloid plaques could not be detected with our 7T MRI without a contrast agent.

This Gd staining protocol enabled the detection of amyloid plaques by both in vivo and in vitro μMRI in APP/PS1 mice brain from as early as 6 months of age. At this age, cortical and hippocampal plaques contain no or low levels of endogenous iron and are thus weakly detected by μMRI without contrast agent. The Gd staining method was sensitive enough to demonstrate an age-dependent increase of amyloid plaque load and a good correlation between amyloid load measured by μMRI and histology. The underlying mechanisms of contrast enhancement induced by Gd staining could be due to the hydrophilic properties of Gd that prevent it from associ-

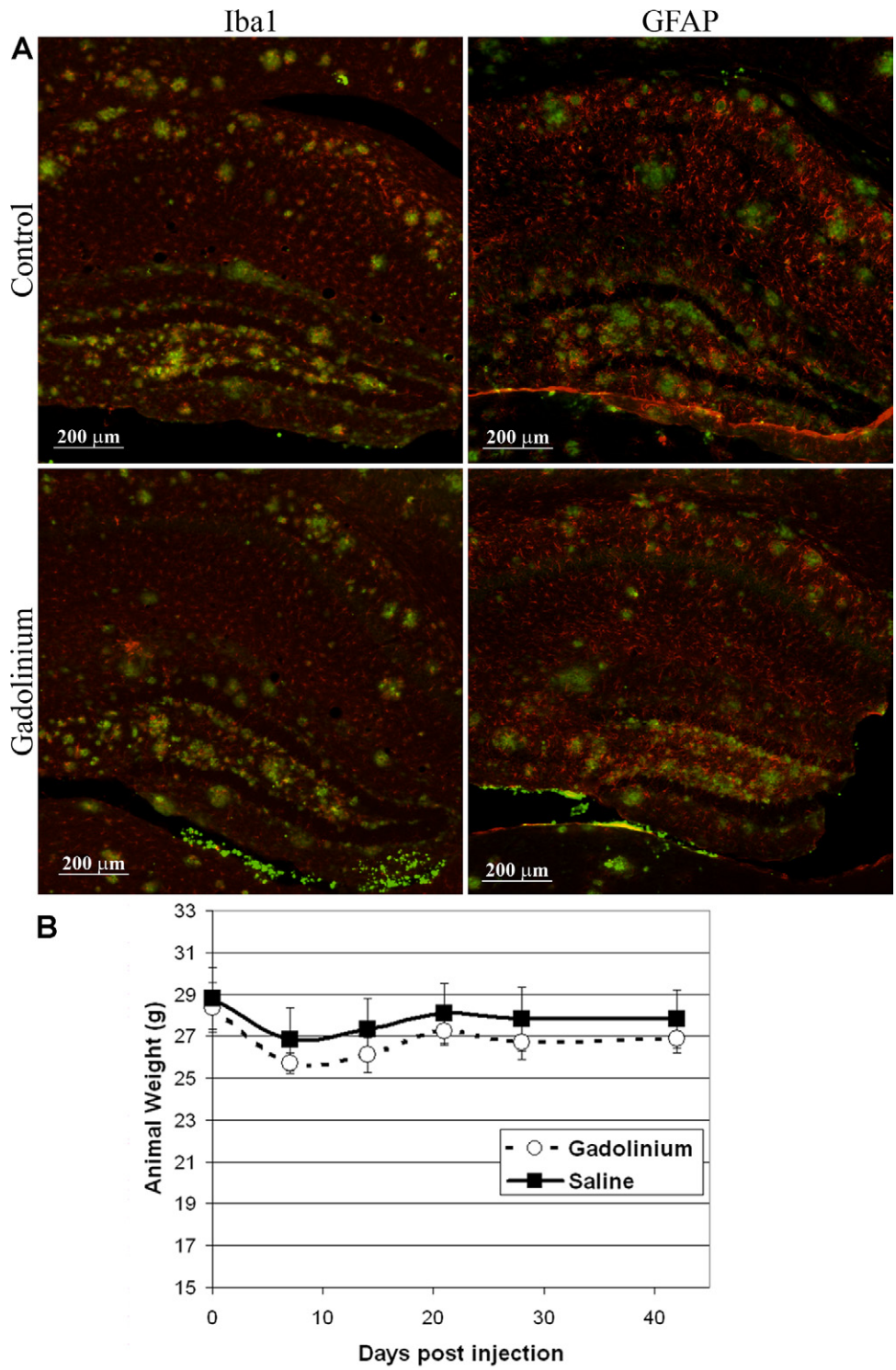

Fig. 6. Evaluation of the effect of gadolinium (Gd) injections on neuroinflammation and on animals' weight. (A-Left panels) Sections stained for microglia (Iba1, red staining) and amyloid (BAM10, green staining) did not show any obvious changes between 8-month-old animals injected twice in the cerebral ventricles (ICV) with Gd (at 3.5 and 8 months, bottom) versus noninjected age-matched animals (top). (A-Right panels) Sections stained for reactive astrocytes (glial fibrillary acidic protein [GFAP], red staining) and amyloid (BAM10, green staining) also did not show any obvious changes between the 2 groups of animals. (B) The animals injected with Gd vs. saline did not show any significant changes of weight over 42 days following injection (Day 0 = injection day).

ating with the highly hydrophobic amyloid plaques. As a result the Gd agent is expected to specifically stain the parenchymal tissue and thereby increase the contrast between the parenchyma and the amyloid deposits. Previous studies have used active or passive Gd staining protocols of postmortem rodent brains to improve in vitro

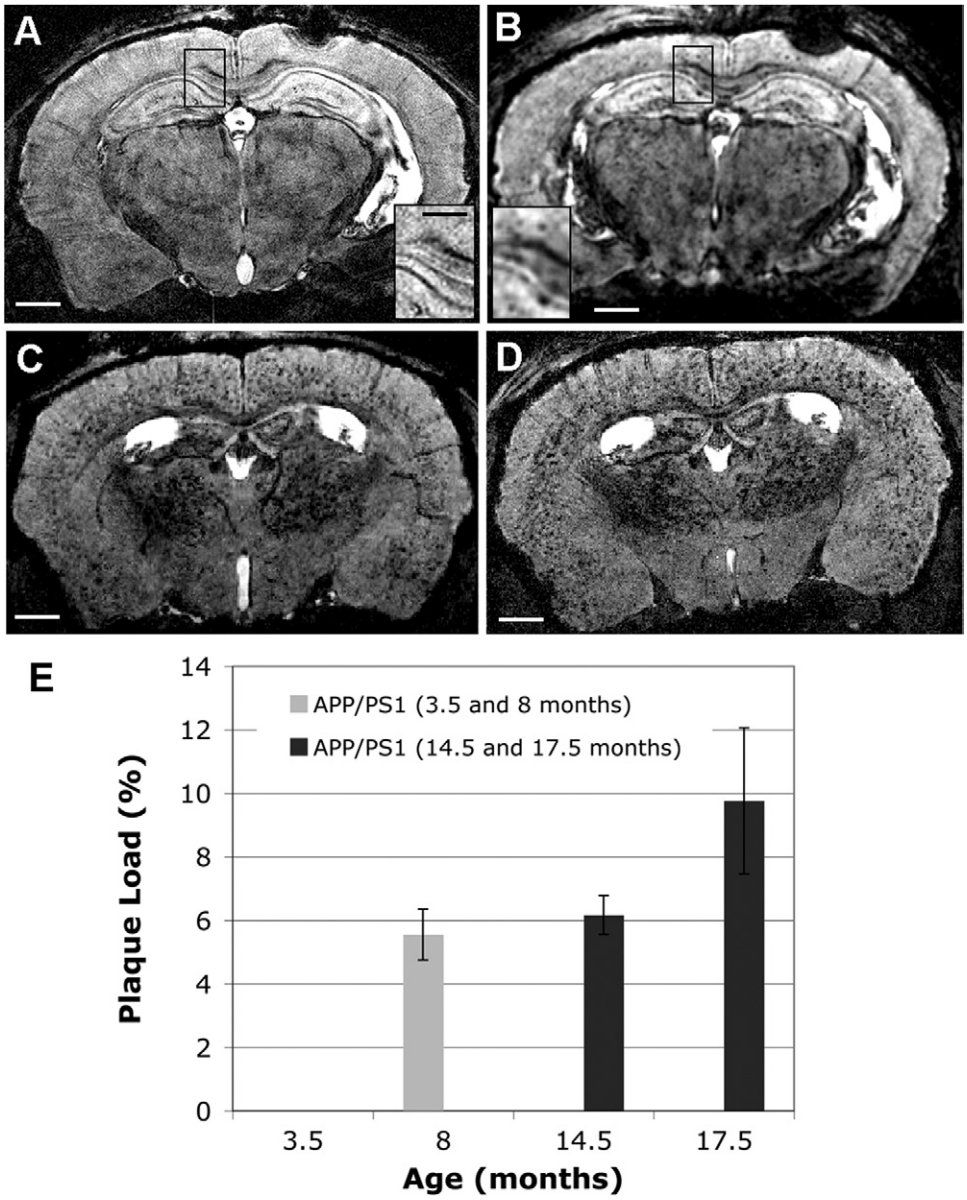

Fig. 7. Longitudinal study of 2 APP/PS1 mice injected at 2 time points with gadolinium (Gd) (datasets recorded on the Varian system with the imaging parameters described in the methods section). One was injected and scanned at 3.5 months (A) then at 8 months (B); and another mouse was injected at 14.5 months (C) then at 17.5 months (D). Notice the comparable signal-to-noise ratio (SNR) between the first (A and C) and the second injections (B and D). Amyloid plaques can clearly be seen in the cortex at 8 months (B and close-up view in B), 14.5 months, and 17.5 months, but not at 3.5 months. Scale bars = 1 mm. The close-up views in (A) and (B) are magnified 2× (scale bar = 500 μm). The bar graph in (E) shows the plaque load measured in these 2 mice: 0% at 3.5 months increased to 5.5% at 8 months, and 6.2% at 14.5 months increased to 9.7% at 17.5 months. The error bars represent the standard deviations.

μMR imaging of brain samples (Dhenain et al., 2006; Kappeler et al., 2007). Here we provide the first demonstration that Gd staining can be used to enhance the detection of amyloid plaques by in vivo μMR imaging.

Previous attempts to visualize amyloid plaques in transgenic mice by μMRI without contrast agents have been limited by the fact that the ability to detect individual plaques is dependent on the relaxation effects mediated by the presence of iron associated with the plaques. Because iron accumulation and its association with plaques are mainly observed in old animals, this has hindered the ability to quantify the age-dependent accumulation of amyloid plaques in the brain. Other studies have used targeted contrast agents in combination with agents, such as mannitol and putrescine (Poduslo et al., 2002; Wadghiri et al., 2003) to open the BBB to deliver agents via intravascular injections, but this approach still requires extensive validation. Here we show that stereotaxic intraventricular injection of a nontargeted contrast agent can be used to detect amyloid plaques in the brain by in vivo μMRI.

Our results show that Gd staining enables the detection of amyloid plaques by μMRI that contain no or little iron. It is therefore possible to use this technique to detect the progression of amyloid pathology at different ages and to evaluate the ability of antiamyloid therapies to inhibit or slow down the age-dependent accumulation of amyloid plaques. Although several targeted contrast agents based on the chemical synthesis of Gd or iron agents linked to molecules targeting amyloid plaques (Poduslo et al., 2002; Sigurdsson et al., 2008; Wadghiri et al., 2003) are under development, our method has the advantage of using a commercially available and inexpensive contrast agent (gadoterate meglumine; Gd-DOTA; DOTAREM®). In addition, such a nonspecific contrast agent is not expected to interfere with amyloidogenesis, unlike specific contrast agents composed of Aβ fragments (Wadghiri et al., 2003) or Aβ antibodies (Poduslo et al., 2002), that are consequently less suitable for longitudinal follow-up studies and the assessment of pharmacological treatments.

There are also several possibilities to further refine this protocol both at the level of contrast agent administration and at the level of imaging protocols. Regarding contrast agent administration, one limitation of our approach is that it requires intracerebroventricular injection of the agent to bypass the blood-brain barrier. Indeed, in normal conditions, after intravenous (IV) injection, gadolinium contrast agents do not extravasate from the bloodstream into the interstitial space because of the blood-brain barrier (Giesel et al., 2010). BBB breakdown can lead to a leakage of gadolinium contrast agents into the brain. Such BBB breakdown can occur in pathological condition and several studies, but not all (Bourasset et al., 2009), have shown BBB alterations in transgenic mouse models of AD (Cirrito et al., 2005; Ujiie et al., 2003). However, in our mice, BBB damage, if any, was not severe enough to allow a significant leakage of gadolinium contrast agents into the brain (data not shown). Several protocols, based on ultrasound (Hynynen et al., 2005; Raymond et al., 2008) or drug carriers such as solid lipid nanoparticles (Peira et al., 2003) are currently being developed to artificially open the BBB, including in humans (Deffieux and Konofagou, 2010; Madsen and Hirschberg, 2010) and allow the passage of intravenously injected MRI contrast agents into the brain (Howles et al., 2010). Future work will have to implement these protocols for amyloid plaque detection. Imaging protocols can also be refined to improve the quality of the in vivo images, including the use of cardiorespiratory triggering (Jack et al., 2004) or sequence optimization (Chamberlain et al., 2009) and the use of a more efficient MR coil (see Fig. 5), such as a small diameter birdcage with a high filling factor or a surface coil closely positioned on the head of the animal. In addition, the availability of very high-field magnets (14–21 Tesla) in several laboratories will allow higher spatial resolution and faster scans for routine screening of animal cohorts.

In conclusion, we have shown that in vivo and in vitro Gd staining enables the detection of amyloid plaques in the brain of transgenic mice by μMRI. This approach can repeatedly be used to follow the progression of AD in the same animal and has therefore the potential to evaluate the activity of amyloid-lowering therapeutic strategies in longitudinal studies at the preclinical level. The contrast enhancement technique used also has the potential to be applied to other types of neuropathologies such as multiple sclerosis (MacKenzie-Graham et al., 2009) or neurodevelopmental alterations (Badea et al., 2007) to enable significant increases in the sensitivity of in vivo microscopic imaging of brain lesions in animal models. The translation to the clinic, to detect Aβ plaques in human AD brains, should be possible by developing similar contrast agents that can cross the BBB.

Disclosure statement

None of the authors have any actual or potential conflict of interest to declare.

All animal experiments were conducted in accordance with ethical standards of the statutory order 87 848 (October 13, 1987) of the French Ministry of Agriculture (authorizations 91-326).

Acknowledgements

Our work was supported by Medicen (Pôle de compétitivité Île-de-France, TransAl program), the France-Alzheimer association, the France-Berkeley fund, and the NIH R01-AG020197. We thank E. Bourrin from Servier and C. Jan from CEA MIRCen for participation in the histological studies.

References

Badea, A., Nicholls, P.J., Johnson, G.A., Wetsel, W.C., 2007. Neuroanatomical phenotypes in the reeler mouse. Neuroimage 34, 1363–1374.

Benveniste, H., Kim, K., Zhang, L., Johnson, G.A., 2000. Magnetic resonance microscopy of the C57BL mouse brain. Neuroimage 11, 601–611.

Berghorn, K.A., Bonnett, J.H., Hoffman, G.E., 1994. cFos immunoreactivity is enhanced with biotin amplification. J. Histochem. Cytochem. 42, 1635–1642.

Blanchard, V., Moussaoui, S., Czech, C., Touchet, N., Bonici, B., Planche, M., Canton, T., Jedidi, I., Gohin, M., Wirths, O., Bayer, T.A., Langui, D., Duyckaerts, C., Tremp, G., Pradier, L., 2003. Time sequence of maturation of dystrophic neurites associated with Abeta deposits in APP/PS1 transgenic mice. Exp. Neurol. 184, 247–263.

Bourasset, F., Ouellet, M., Tremblay, C., Julien, C., Do, T.M., Oddo, S., Laferla, F., Calonc, F., 2009. Reduction of the cerebrovascular volume in a transgenic mouse model of Alzheimer's disease. Neuropharmacology, 56, 808–813.

Chamberlain, R., Reyes, D., Curran, G.L., Marjanska, M., Wengenack, T.M., Poduslo, J.F., Garwood, M., Jack, C.R., Jr, 2009. Comparison of amyloid plaque contrast generated by T2-weighted, T2*-weighted, and susceptibility-weighted imaging methods in transgenic mouse models of Alzheimer's disease, Magn. Reson. Med. 61, 1158–1164.

Cirrito, J.R., Deane, R., Fagan, A.M., Spinner, M.L., Parsadanian, M., Finn, M.B., Jiang, H., Prior, J.L., Sagare, A., Bales, K.R., Paul, S.M., Zlokovic, B.V., Piwnica-Worms, D., Holtzman, D.M., 2005. P-glyco-

protein deficiency at the blood–brain barrier increases amyloid-beta deposition in an Alzheimer disease mouse model. J. Clin. Invest. 115, 3285–3290.

Deffieux, T., Konofagou, E.E., 2010. Numerical study of a simple transcranial focused ultrasound system applied to blood-brain barrier opening. IEEE Transact. Ultrason. Ferroelectr. Freq. Control 57, 2637–2653.

Delatour, B., Epelbaum, S., Petiet, A., Dhenain, M., 2010. In vivo imaging biomarkers in mouse models of Alzheimer's disease: Are we lost in translation or breaking through? Int. J. Alzheimers Dis., pii: 604853.

Delatour, B., Guégan, M., Volk, A., Dhenain, M., 2006. In vivo MRI and histological evaluation of brain atrophy in APP/PS1 transgenic mice. Neurobiol. Aging 27, 835–847.

Dhenain, M., 2008. Preclinical MRI and NMR biomarkers of Alzheimer's disease: concepts and applications. Magnetic Resonance Insights, 275–291.

Dhenain, M., Delatour, B., Walczak, C., Volk, A., 2006. Passive staining: A novel ex vivo MRI protocol to detect amyloid deposits in mouse models of Alzheimer's disease. Magn. Reson. Med. 55, 687–693.

Dhenain, M., El Tannir El Tayara, N., Wu, T.-D., Guegand, M., Volk, A., Quintana, C., Delatour, B., 2009. Characterization of in vivo MRI detectable thalamic amyloid plaques from APP/PS1 mice. Neurobiol. Aging 30, 41–53.

Dhenain, M., Privat, N., Duyckaerts, C., Jacobs, R.E., 2002. Senile plaques do not induce susceptibility effects in T2*-weighted MR microscopic images. NMR Biomed. 15, 197–203.

El Tannir El Tayara, N., Delatour, B., Le Cudennec, C., Guégan, M., Volk, A., Dhenain, M., 2006. Age-related evolution of amyloid burden, iron load, and MR relaxation times in a transgenic mouse model of Alzheimer's disease. Neurobiol. Dis. 22, 199–208.

El Tannir El Tayara, N., Volk, A., Dhenain, M., Delatour, B., 2007. Transverse relaxation time reflects brain amyloidosis in young APP/PS1 transgenic mice. Magn. Reson. Med. 58, 179–184.

Giesel, F.L., Mehndiratta, A., Essig, M., 2010. High-relaxivity contrast-enhanced magnetic resonance neuroimaging: a review. Eur. Radiol. 20, 2461–2474.

Higuchi, M., Iwata, N., Matsuba, Y., Sato, K., Sasamoto, K., Saido, T.C., 2005. 19F and 1H MRI detection of amyloid beta plaques in vivo. Nat. Neurosci. 8, 527–533.

Hintersteiner, M., Enz, A., Frey, P., Jaton, A.L., Kinzy, W., Kneuer, R., Neumann, U., Rudin, M., Staufenbiel, M., Stoeckli, M., Wiederhold, K.H., Gremlich, H.U., 2005. In vivo detection of amyloid-beta deposits by near-infrared imaging using an oxazine-derivative probe. Nat. Biotechnol. 23, 577–583.

Howles, G.P., Bing, K.F., Qi, Y., Rosenzweig, S.J., Nightingale, K.R., Johnson, G.A., 2010. Contrast-enhanced in vivo magnetic resonance microscopy of the mouse brain enabled by noninvasive opening of the blood–brain barrier with ultrasound. Magn. Reson. Med. 64, 995–1004.

Hynynen, K., McDannold, N., Sheikov, N.A., Jolesz, F.A., Vykhodtseva, N., 2005. Local and reversible blood–brain barrier disruption by noninvasive focused ultrasound at frequencies suitable for trans-skull sonications. Neuroimage 24, 12–20.

Jack, C.R., Jr, Garwood, M., Wengenack, T.M., Borowski, B., Curran, G.L., Lin, J., Adriany, G., Gröhn, O.H., Grimm, R., Poduslo, J.F., 2004. In vivo visualization of Alzheimer's amyloid plaques by magnetic resonance imaging in transgenic mice without a contrast agent. Magn. Reson. Med. 52, 1263–1271.

Jack, C.R., Jr, Wengenack, T.M., Reyes, D.A., Garwood, M., Curran, G.L., Borowski, B.J., Lin, J., Preboske, G.M., Holasek, S.S., Adriany, G., Poduslo, J.F., 2005. In vivo magnetic resonance microimaging of individual amyloid plaques in Alzheimer's transgenic mice. J. Neurosci. 25, 10041–10048.

Johnson, G.A., Cofer, G.P., Gewalt, S.L., Hedlund, L.W., 2002. Morphologic phenotyping with MR microscopy: The visible mouse. Radiology 222, 789–793.

Kappeler, C., Dhenain, M., Phan, D., Tuy, F., Saillour, Y., Marty, S., Fallet-Bianco, C., Souville, I., Souil, E., Pinard, J.-M., Meyer, G., Encha-Razavi, F., Volk, A., Beldjord, C., Chelly, J., Francis, F., 2007. MRI and histological studies of corpus callosal and hippocampal abnormalities linked to doublecortin deficiency. J. Comp. Neurol. 500, 239–254.

Klunk, W.E., Engler, H., Nordberg, A., Wang, Y., Blomqvist, G., Holt, D.P., Bergström, M., Savitcheva, I., Huang, G.F., Estrada, S., Ausén, B., Debnath, M.L., Barletta, J., Price, J.C., Sandell, J., Lopresti, B.J., Wall, A., Koivisto, P., Antoni, G, Mathis, C.A., Langstrom, B., 2004. Imaging brain amyloid in Alzheimer's disease with Pittsburgh Compound-B. Ann. Neurol. 55, 306–319.

Klunk, W.E., Lopresti, B.J., Ikonomovic, M.D., Lefterov, I.M., Koldamova, R.P., Abrahamson, E.E., Debnath, M.L., Holt, D.P., Huang, G.F., Shao, L., DeKosky, S.T., Price, J.C., Mathis, C.A., 2005. Binding of the positron emission tomography tracer Pittsburgh compound-B reflects the amount of amyloid-beta in Alzheimer's disease brain but not in transgenic mouse brain. J. Neurosci. 25, 10598–10606.

MacKenzie-Graham, A., Tiwari-Woodruff, S.K., Sharma, G., Aguilar, C., Vo, K.T., Strickland, L.V., Morales, L., Fubara, B., Martin, M., Jacobs, R.E., Johnson, G.A., Toga, A.W., Voskuhl, R.R., 2009. Purkinje cell loss in experimental autoimmune encephalomyelitis. Neuroimage 48, 637–651.

Madsen, S.J., Hirschberg, H., 2010. Site-specific opening of the blood–brain barrier. J. Biophoton. 3, 356–367.

Maeda, J., Ji, B., Irie, T., Tomiyama, T., Maruyama, M., Okauchi, T., Staufenbiel, M., Iwata, N., Ono, M., Saido, T.C., Suzuki, K., Mori, H., Higuchi, M., Suhara, T., 2007. Longitudinal, quantitative assessment of amyloid, neuroinflammation, and anti-amyloid treatment in a living mouse model of Alzheimer's disease enabled by positron emission tomography. J. Neurosci. 27, 10957–10968.

Meadowcroft, M.D., Connor, J.R., Smith, M.B., Yang, Q.X., 2009. MRI and histological analysis of beta-amyloid plaques in both human Alzheimer's disease and APP/PS1 transgenic mice. J. Magn. Reson. Imaging 29, 997–1007.

Nordberg, A., 2007. Amyloid imaging in Alzheimer's disease. Curr. Opin. Neurol. 20, 398–402.

Paxinos, G., Franklin, K.B.J., 2001. The Mouse Brain in Stereotaxic Coordinates, second ed. Academic Press, San Diego.

Peira, E., Marzola, P., Podio, V., Aime, S., Sbarbati, A., Gasco, M.R., 2003. In vitro and in vivo study of solid lipid nanoparticles loaded with superparamagnetic iron oxide. J. Drug Target. 11, 19–24.

Petiet, A., Hedlund, L., Johnson, G.A., 2007. Staining methods for magnetic resonance microscopy of the rat fetus. J. Magn. Reson. Imaging 25, 1192–1198.

Poduslo, J.F., Wengenack, T.M., Curran, G.L., Wisniewski, T., Sigurdsson, E.M., Macura, S.I., Borowski, B.J., Jack, C.R., Jr, 2002. Molecular targeting of Alzheimer's amyloid plaques for contrast-enhanced magnetic resonance imaging. Neurobiol. Dis. 11, 315–329.

Raymond, S.B., Treat, L.H., Dewey, J.D., McDannold, N.J., Hynynen, K., Bacskai, B.J., 2008. Ultrasound enhanced delivery of molecular imaging and therapeutic agents in Alzheimer's disease mouse models. PLoS One 3, e2175.

Sigurdsson, E.M., Wadghiri, Y.Z., Mosconi, L., Blind, J.A., Knudsen, E., Asuni, A., Scholtzova, H., Tsui, W.H., Li, Y., Sadowski, M., Turnbull, D.H., de Leon, M.J., Wisniewski, T., 2008. A non-toxic ligand for voxel-based MRI analysis of plaques in AD transgenic mice. Neurobiol. Aging 29, 836–847.

Ujiie, M., Dickstein, D.L., Carlow, D.A., Jefferies, W.A., 2003. Blood-brain barrier permeability precedes senile plaque formation in an Alzheimer disease model. Microcirculation 10, 463–470.

Wadghiri, Y.Z., Sigurdsson, E.M., Sadowski, M., Elliott, J.I., Li, Y., Scholtzova, H., Tang, C.Y., Aguilnaldo, G., Pappolla, M., Duff, K., Wisniewski, T.M., Turnbull, D.H., 2003. Detection of Alzheimer's amyloid in transgenic mice using magnetic resonance microimaging. Magn. Reson. Med. 50, 293–302.